Science Advances
AAAS

Supplementary Materials for

The mechanosensitive Piezo1 channel controls endosome trafficking for an efficient cytokinetic abscission

Julia Carrillo-Garcia, Víctor Herrera-Fernández, Selma A. Serra, Fanny Rubio-Moscardo, Marina Vogel-Gonzalez, Pablo Doñate-Macian, Covadonga F. Hevia, Cristina Pujades, Miguel A. Valverde*

*Corresponding author. Email: miguel.valverde@upf.edu

Published 29 October 2021, *Sci. Adv.* **7**, eabi7785 (2021)
DOI: 10.1126/sciadv.abi7785

This PDF file includes:

Fig. S1

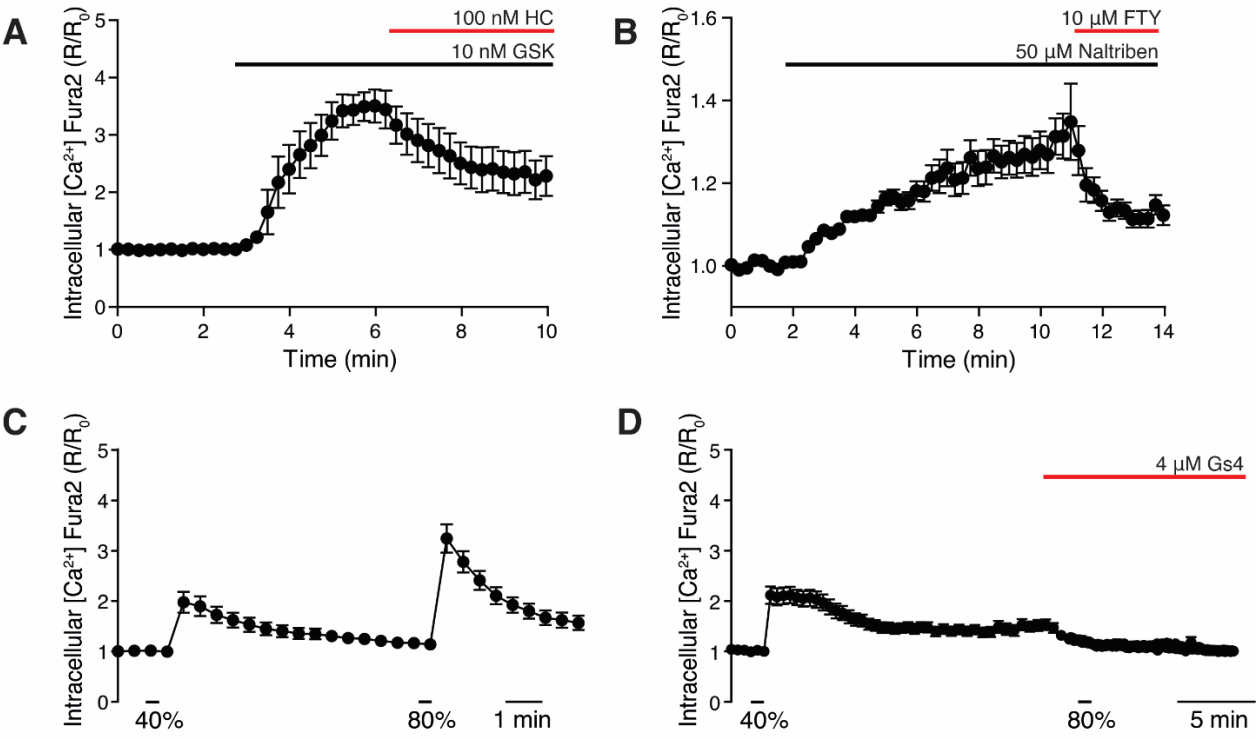

Fig. S1. Functional characterization of mechanosensitive ion channels in HMEC. (**A**) Changes in intracellular [Ca^{2+}] (indicated by normalized fura-2 ratios) in HMEC after perfusion with the TRPV4 activator GSK1016790A followed by addition of the inhibitor HC067047 at the indicated concentrations (N=26). (**B**) Changes in intracellular [Ca^{2+}] in HMEC after perfusion with the TRPM7 activator naltriben followed by addition of the inhibitor FTY720 at the indicated concentrations (N=29). (**C**) Changes in intracellular [Ca^{2+}] in HMEC after application of two consecutive uniaxial stretching pulses of 40% and 80% of the initial chamber length (N=55). (**D**) Changes in intracellular [Ca^{2+}] in HMEC after application of two consecutive uniaxial stretching pulses, the second after addition of 4 mM GsMTx4 (N=38). Traces are means ± SEM.

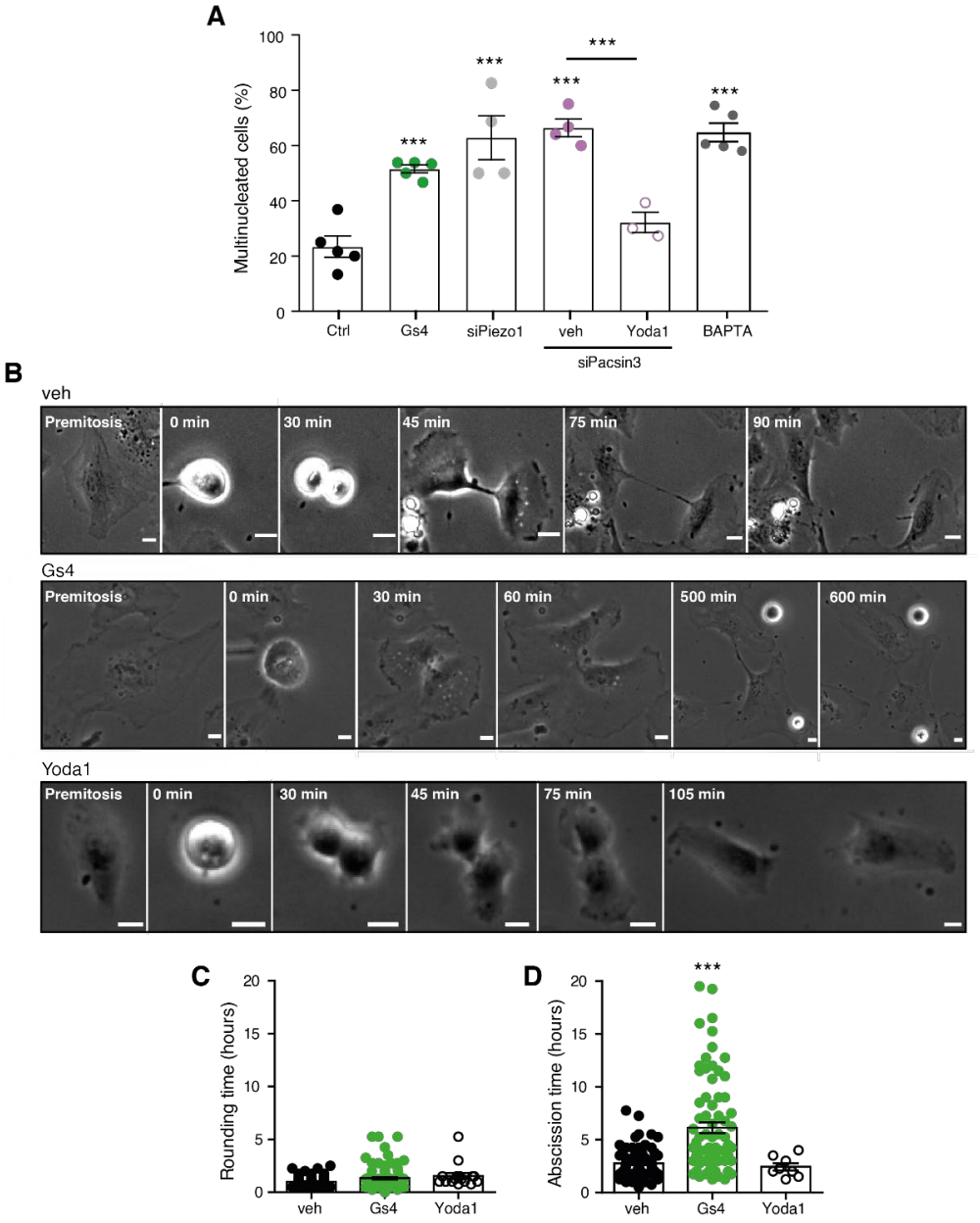

Fig. S2. Quantitative analysis of cytokinesis. (A) Multinucleation of HMEC transfected with the indicated siRNAs and/or treated with the Piezo1 inhibitor (GsMTx4, 1 μM). Per sample, >47 cells were monitored for ≥ 2 nuclei (multinucleation). (**B**) Selected frames from time-lapse videos of HMEC exposed to vehicle (top) of GsMTx4 (bottom). Scale bar=15 μm. (**C**) Quantification of the time to enter mitosis (rounding time) following release from synchronization. At the time cell round up time is set to t=0. (**D**) Quantification of abscission time, defined as the time from rounding (time=0) to the generation of two independent daughter cells. Bars represent mean ± SEM of the number of cells (or experiments repeats in A) shown in each bar. Statistical significance versus control was determined using ANOVA followed by Bonferroni's post hoc (A) o Kruskal-Wallis followed by Dunn's post hoc (C,D). *** P<0.001.

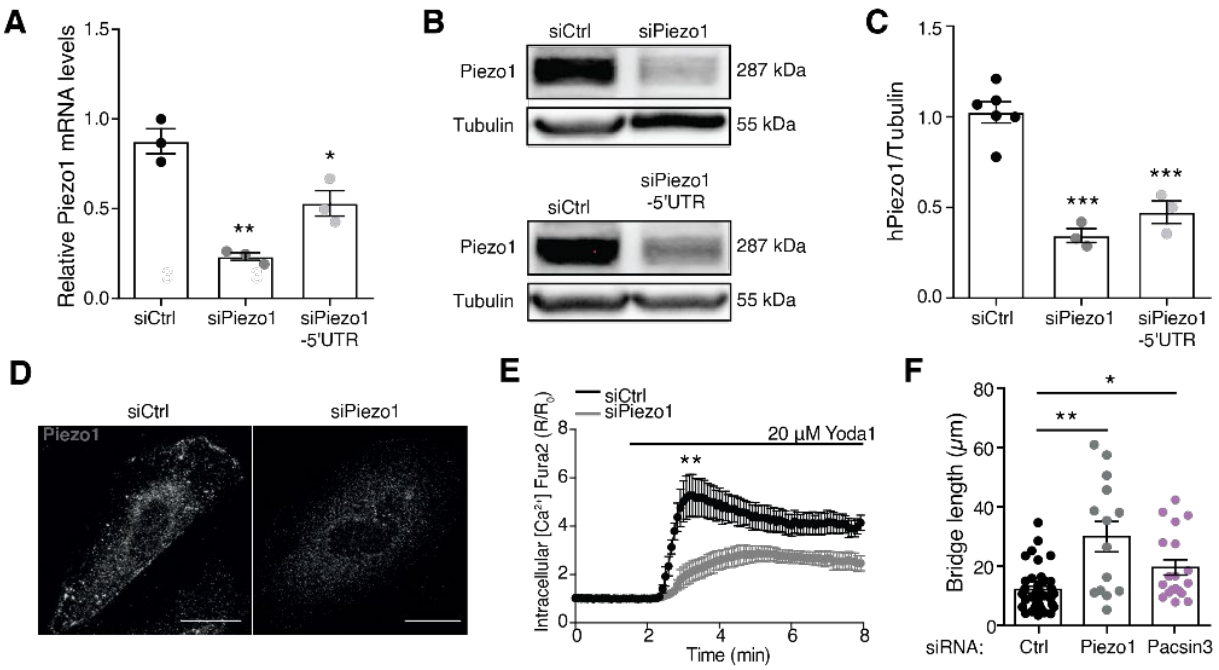

Fig. S3. Knockdown of Piezo1 in HMEC. (**A**) Quantitative real-time PCR of Piezo1 expression in HMEC transfected with siControl, siPiezo1 or siPiezo1-5'UTR. (**B**) Western blot analysis of Piezo1 and α-tubulin obtained from extracts of HMEC transfected with siControl, siPiezo1 or siPiezo1-5'UTR. (**C**) Quantification of the western blot bands. (**D**) Immunofluorescence confocal microscopy images of Piezo1 in HMEC. Note the strong reinforcement of Piezo1 signal at the cell boundary of control siRNA transfected cells and the absence of Piezo1 signal at the cell boundary in siPiezo1 transfected HMEC. Scale bar=10 µm. (**E**) Changes in intracellular [Ca^{2+}] in HMEC transfected with siControl or siPiezo1 and exposed to the Piezo1 activator Yoda1 (10 µM). Note the marked reduction in the response of siPiezo1 transfected cells. Data are mean ± SEM of 43 siControl and 38 siPiezo1 transfected cells. (**F**) Quantification of the length of the ICB in HMEC transfected with control siRNA, siPiezo1 or siPacsin3. Statistical significance versus control was determined using ANOVA followed by Bonferroni's post hoc test, Student's unpaired t test (E) or Kruskal-Wallis followed by Dunn's post hoc (F).

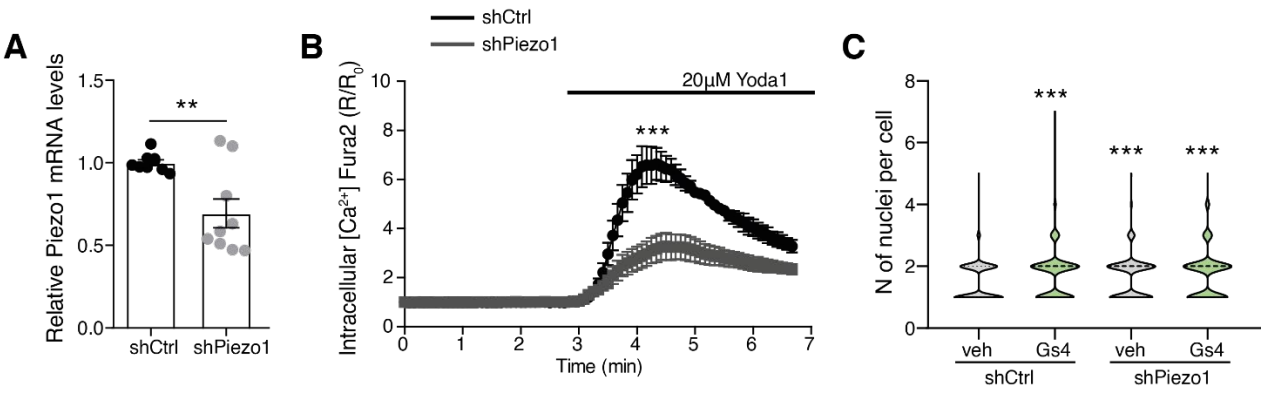

Fig. S4. Piezo1 knockdown induces multinucleation in breast cancer cells. (**A**) Quantitative real-time PCR of Piezo1 expression in shControl and shPiezo1 MDA-MB-231-BrM2 cells. (**B**) Changes in intracellular [Ca^{2+}] in shControl and shPiezo1 MDA-MB-231-BrM2 cells exposed to Yoda1 (20 μM). Note the marked reduction in the response to Yoda1 of shPiezo1 transfected cells. Data are mean ± SEM of 80 shControl and 80 shPiezo1 cells. (**C**) Number of nucle/cell in shControl treated with vehicle (n=732) or GsMTx4 (n=471) and shPiezo1 MDA-MB-231-BrM2 cells treated with vehicle (n=618) or GsMTx4 (n=376). Statistical significance was determined using a Student's unpaired t test (A, B) or Kruskal-Wallis followed by Dunn's post hoc (C).

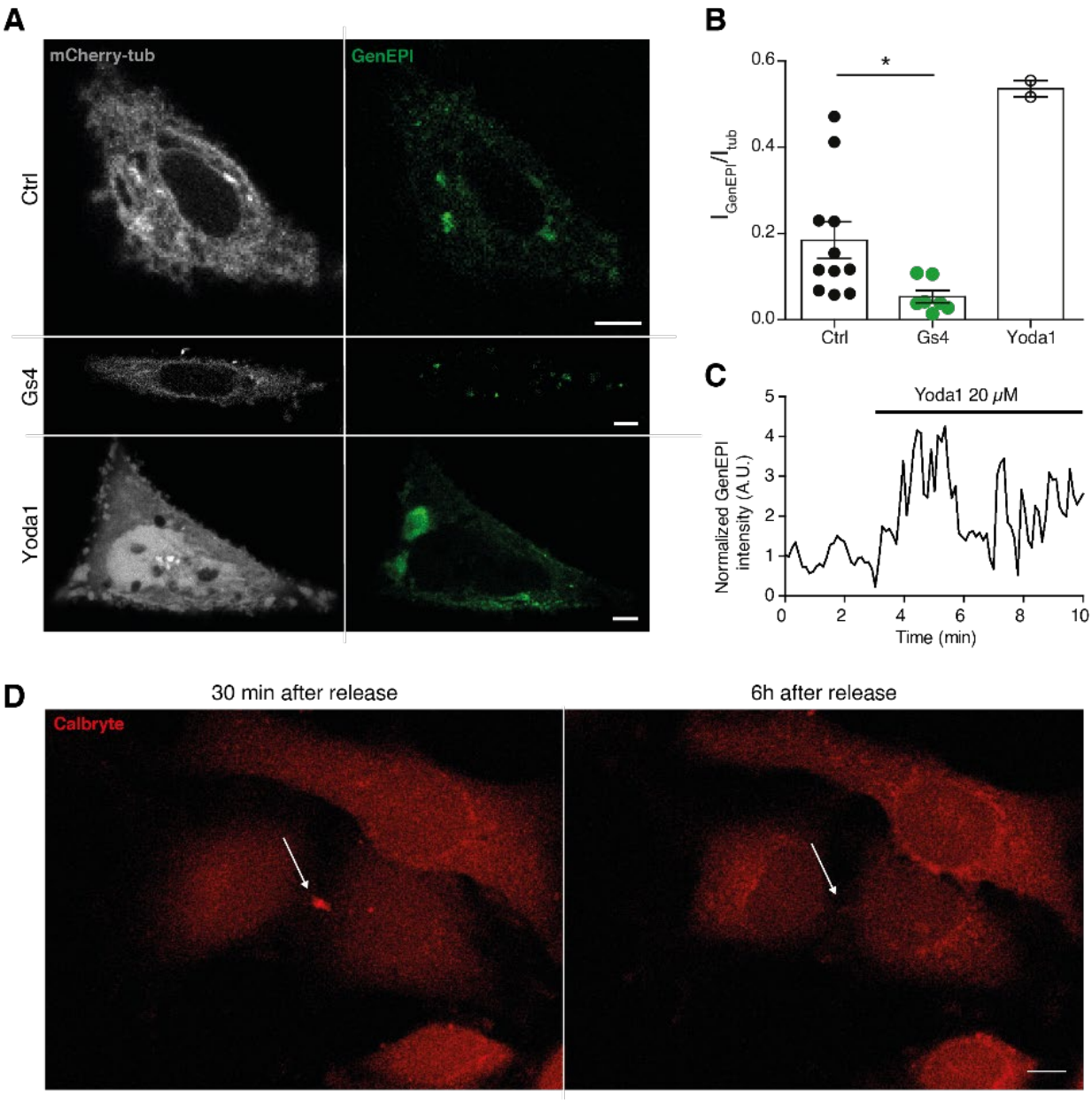

Fig. S5. Activity of the GenEPI fusion protein. (A) Images of cells transfected with the Piezo1-GCaMP fusion protein GenEPI and mCherry-tubulin. Cells were exposed to control, GsMTx4 or Yoda1. Note the increased signal close to the plasma membrane in the Yoda treated cell. (**B**) Quantification of the GenEPI fluorescence signals (reflecting $[Ca^{2+}]$ in the vicinity of the Piezo1 channel) in control cells and those treated with GsMTx4 or Yoda1. Statistical significance versus control was determined using ANOVA followed by Bonferroni's post hoc test (**C**) Time-lapse recording of the GenEPI fluorescence signal in response to Yoda1. (**D**) Images of HeLa cells loaded with the Ca^{2+} indicator, Calbryte™ 630, taken at two different times after release from synchronization. Note the strong Calbryte signal at the intercellular bridge 30 min after release from synchronization. Significant values are respect control condition as determined by Kruskal-Wallis followed by Dunn's post hoc. Scale bar=10 μm.

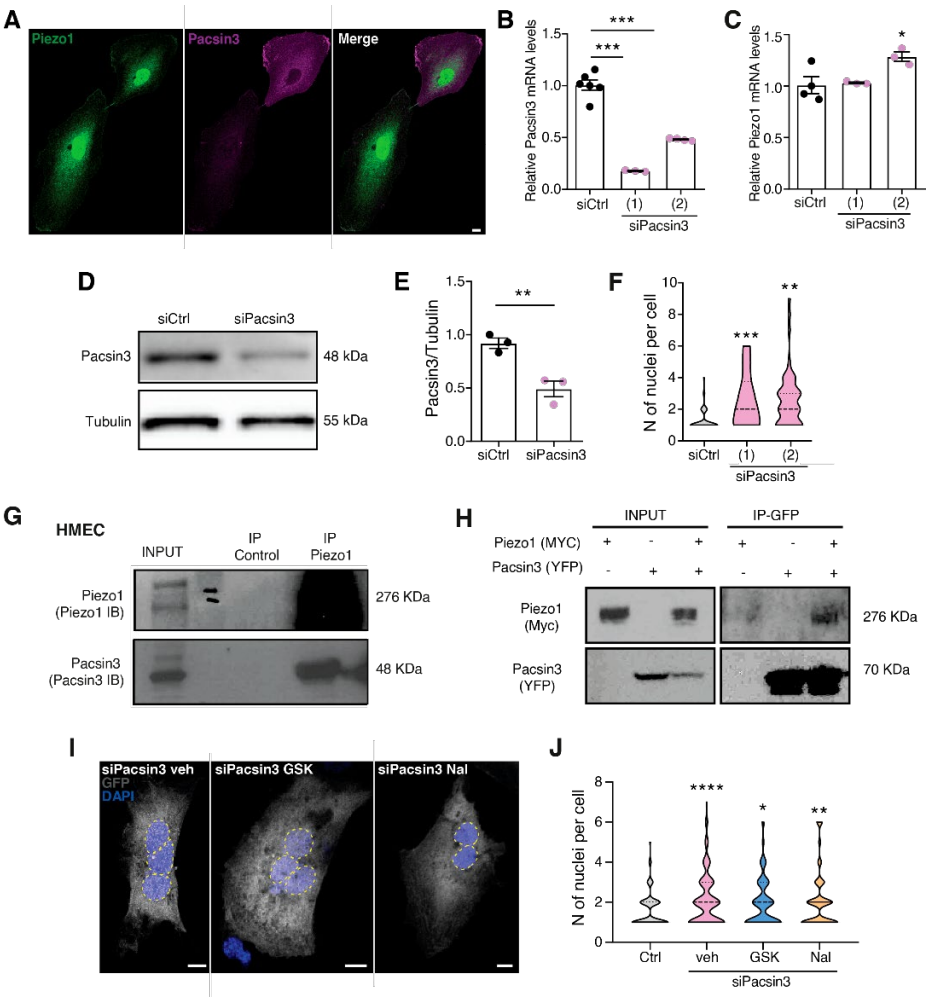

Fig. S6. Pacsin 3 interaction with Piezo1. (**A**) Colocalization of Pacsin3-CFP and endogenous Piezo1 in HMEC during mitosis. Note the clear presence of both Piezo1 and Pcsin3 at the intercellular bridge. (**B**) Quantitative real-time PCR measurements of Pacsin3 mRNA transcript levels in HMEC transfected with siControl or two different siPacsin3. (**C**) Quantitative real-time PCR measurements of Piezo1mRNA transcript levels in HMEC transfected with siControl or two different siPacsin3. (**D**) Western blot analysis of Pacsin3 obtained from extracts of HMEC transfected with siControl or siPacsin3. (**E**) Quantification of the western blot bands. (**F**) Violin plot of the number of nuclei/cell counted in HMEC transfected with siControl (n=57) or two different siRNAs against Pacsin3 (n=57 and n=21). (**G**) Co-immunoprecipitation of endogenous Piezo1 and Pacsin3 in HMEC. (**H**) Co-immunoprecipitaion of Piezo1-myc and Pacsin3-YFP expressed in HEK293 cells. (**I**) Nuclear staining with DAPI (blue) of HMEC transfected with siControl or siPacsin3 and treated with vehicle, GSK101 or naltriben. (**J**) Violin plot of the number of nuclei/cell counted in HMEC transfected with siControl (n= 235) or siPacsin3 and treated with vehicle (n= 191), the TRPV4 activator GSK101 (n= 182) or the TRPM7 activator naltriben (n= 146). Mean ± S.E.M. of the number of cells indicated in each bar. Statistical significance was determined using and ANOVA followed by Dunnett's post hoc test (B,C), Student's unpaired t-test (E) or Kruskal-Wallis followed by Dunn's post hoc (F,J). Bar = 10 μm

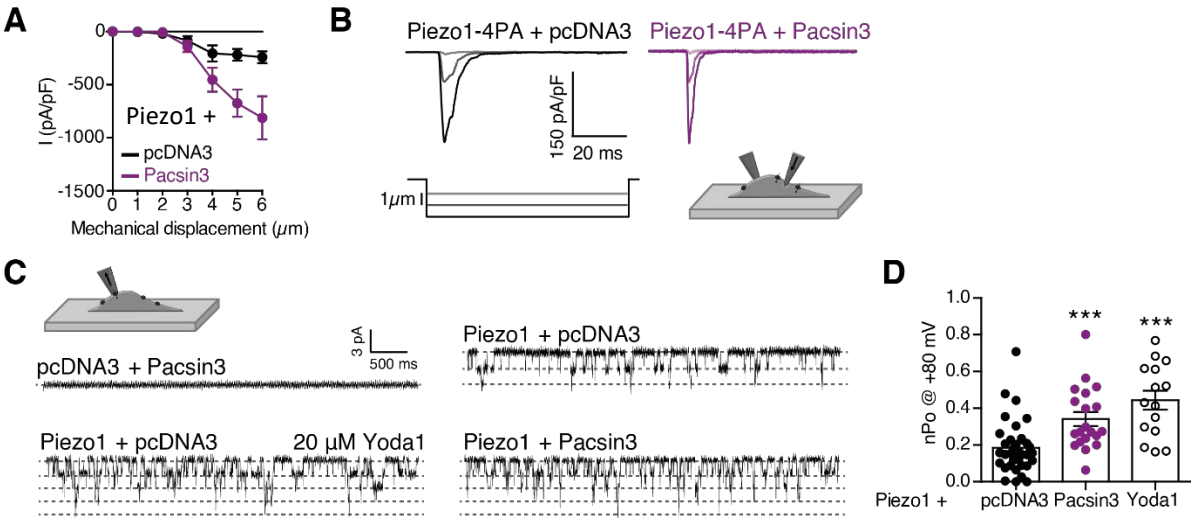

Fig. S7. Electrophysiological recordings of Piezo1 activity. (**A**) Peak current density of whole-cell current recordings of Piezo1 channels heterologously expressed in HEK293 cells with or without the coexpression of Pacsin3. Cells were mechanically stimulated with a blunt pipette under the control of a piezoelectric actuator in steps of 1 μm. Mean ± S.E.M. of 18 cells transfected with Piezo1 and 15 cells transfected with Piezo1 plus Pacsin3. (**B**) Whole-cell recordings obtained from HEK293 cells transfected with Piezo1-4PA alone or with Pacsin3 following stimulation with a series of mechanical steps of 1 μm. (**C**) Cell attached recordings obtained from HEK293 cells transfected with the indicated plasmids and exposed to a negative pressure pulses of -8 mm Hg for 10 sec (Inset illustration). Recordings were carried out immediately after removal of the pressure pulse and in the presence of the Piezo1 activator Yoda1 (bottom left). Note the absence of channel activity in the membrane patch obtained from HEK293 cells expressing Pacsin3 alone. (**D**) Mean open probability (NPo) calculated from cell-attach patches (as shown in C). Mean ± S.E.M. of NPo obtained from the number of patches indicated in each bar. ANOVA followed by Dunnett's post hoc test.

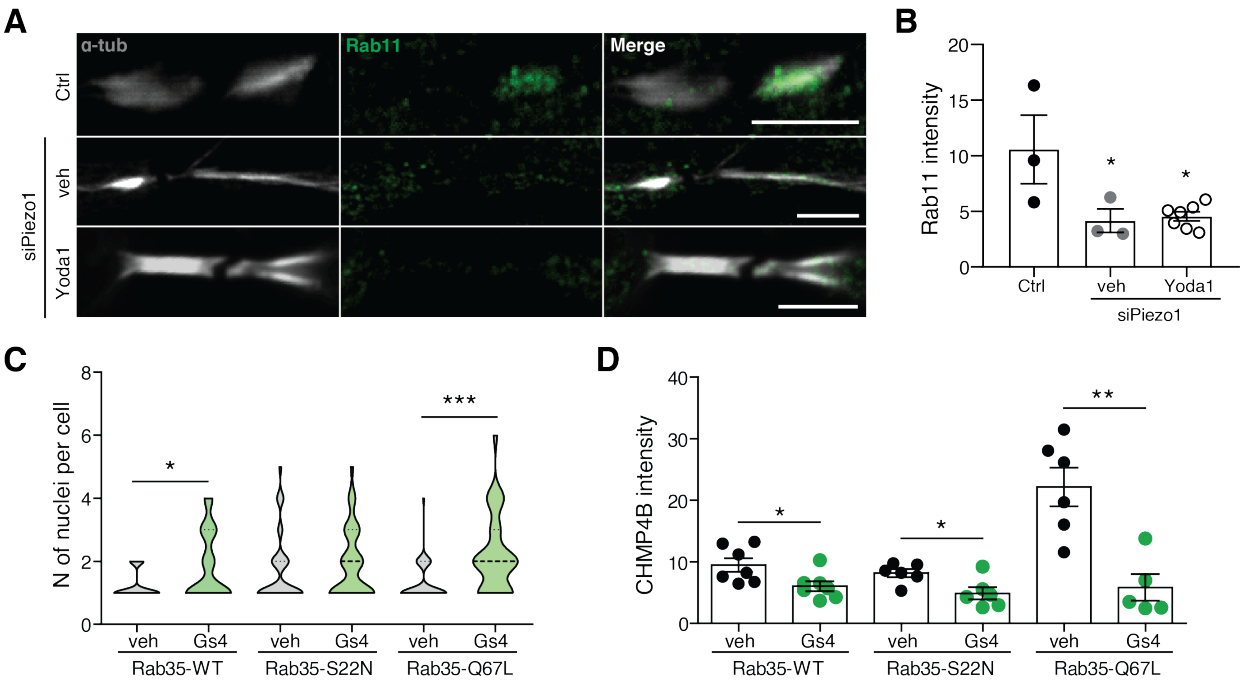

Fig. S8. Role of Rab small GTPases on Piezo1-mediated multinucleation and CHAMP4B localization. (**A**) Immunolocalization of Rab11 at the midbody of siPiezo1 transfected HMEC in the presence/absence of Yoda1. Immunolocalization of a-tubulin in white. Bar= 5 μm. (**B**) Quantification of Rab11 intensity at the ICB in HMEC under the conditions shown. (**C**) number of nuclei/cell in HMEC overexpressing Rab35-WT (vehicle=39, GsMTx4=40), Rab35-S22N (Vehicle=35, GsMTx4=41) or Rab35-Q67L (V.ehicle= 42, GsMTx4=32). (**D**) Quantification of CHMP4B intensity at the ICB in HMEC under the conditions shown. Data are means±SEM. Number of replicas indicated in each graph. Significance was determined using an ANOVA followed by Dunnett's post hoc test (B), Kruskal-Wallis followed by Dunn's post hoc (C) or ANOVA followed by Bonferroni's post hoc test (D)

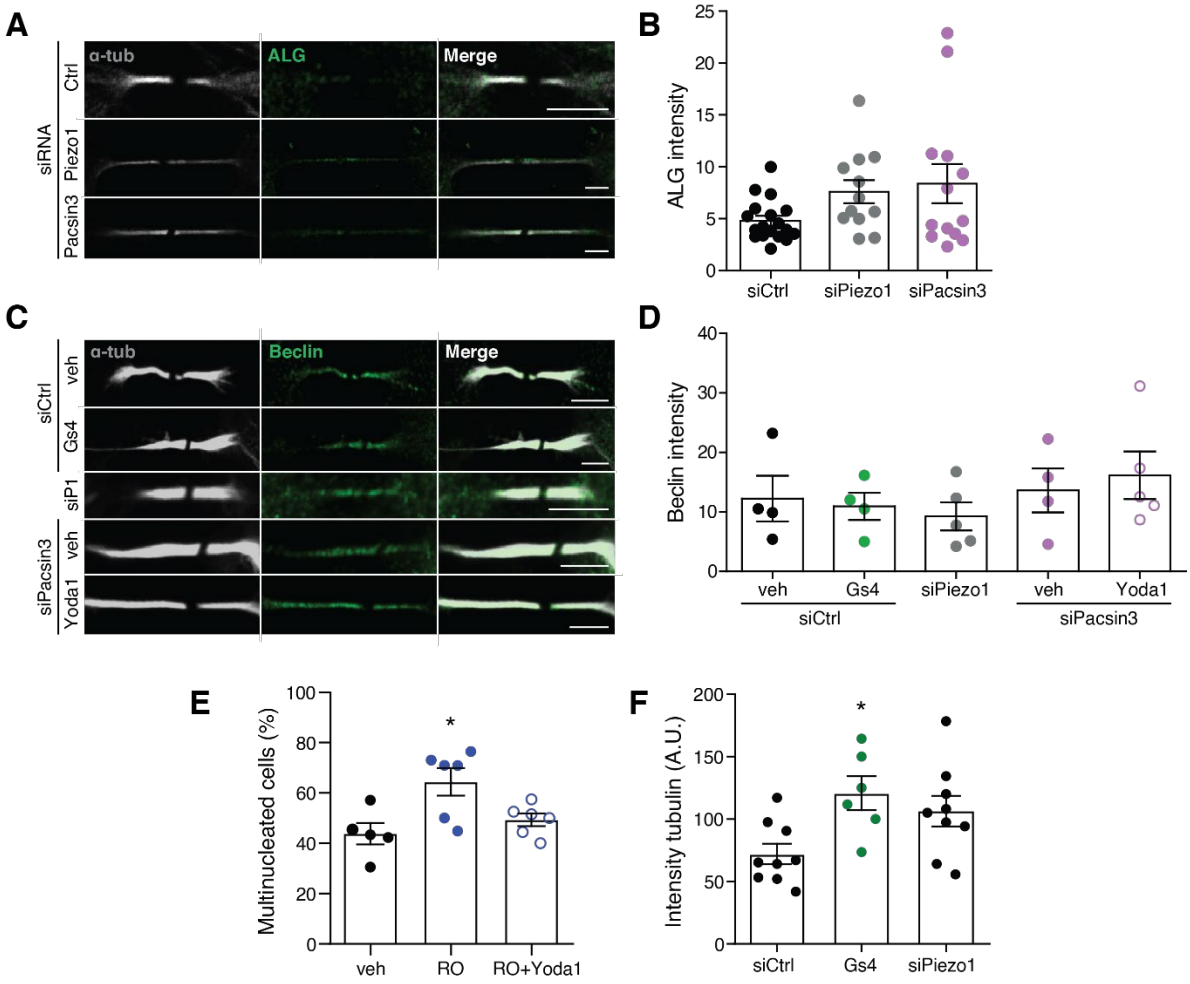

Fig. S9. Effect of Piezo1 on other pathways participating in cytokinesis. Localization (**A**) and quantification (**B**) of ALG-2 signal at the ICB of HMEC under the conditions shown. Localization (**C**) and quantification of Beclin-1 (**D**) signal at the ICB of HMEC under the conditions shown. Data are means ± SEM. Number of replicas indicated in each graph. None of the conditions tested in B and D were significantly different to the control condition as determined by Kruskal-Wallis followed by Dunn's post hoc (B) or ANOVA followed by Dunnett's post hoc test (D). (**E**) Percentage of multinucleated HMEC exposed to vehicle (DMSO) and the Rho kinase inhibitor, Rockout, in the presence or absence of Yoda1. (**F**) Quantification of tubulin intensity in the ICB of HMEC exposed to GsMTx4 or transfected with siControl and siPiezo1. Statistical significance versus control was determined using ANOVA followed by Bonferroni's post hoc (E-F). Scale bar= 5 μm.

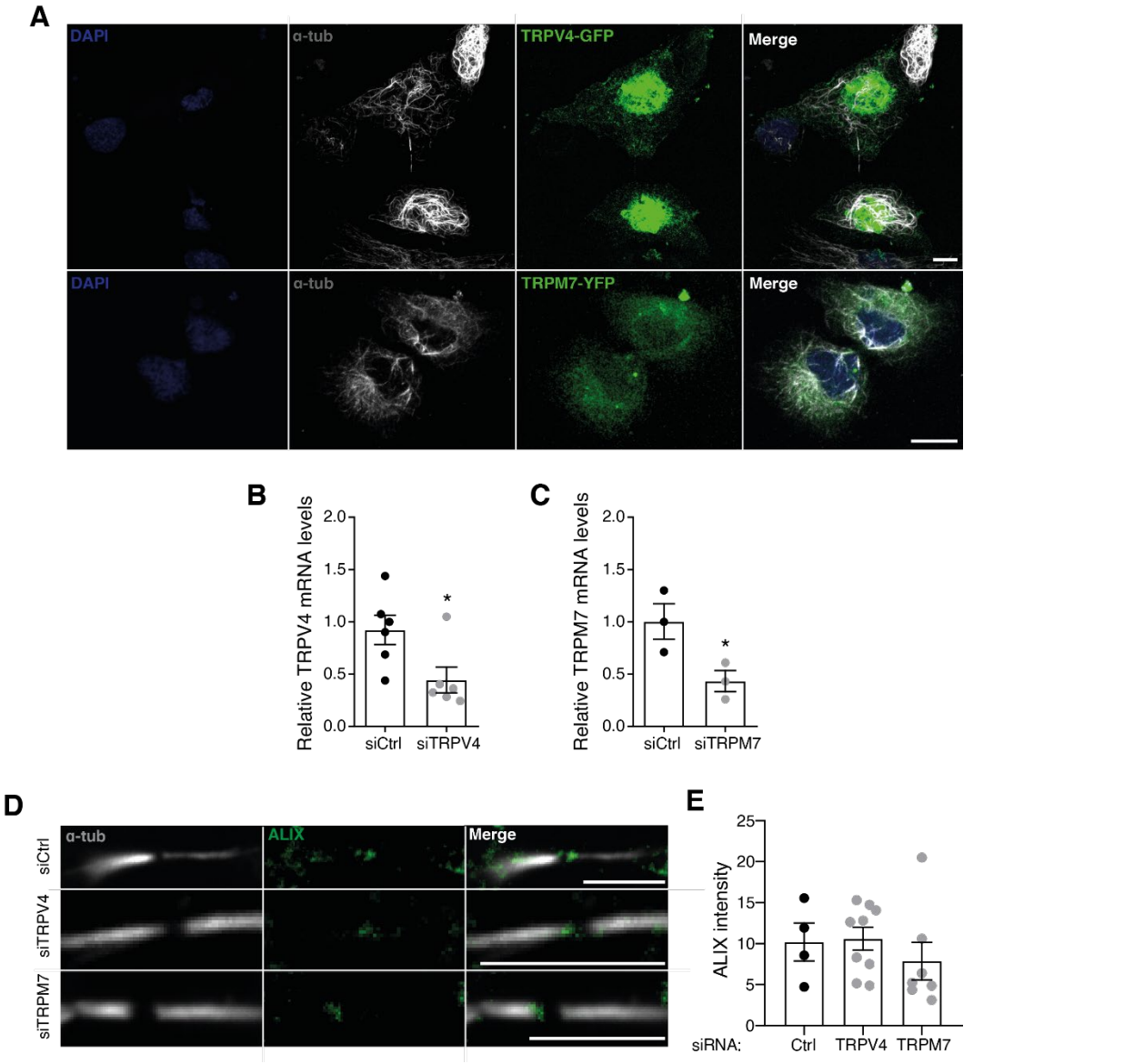

Fig. S10. Effect of TRPV4 or TRPM7 knockdown on localization of ALIX. (A) TRPV4-GFP and TRPM7-YFP localization (green) in late mitosis; anti-α-tubulin staining (white); DAPI nuclear staining (blue). (B) Quantitative PCR measurements of TRPV4 mRNA transcript levels in HMEC transfected with siControl or siTRPV4. (C) Quantitative PCR measurements of TRPV4 mRNA transcript levels in HMEC transfected with siControl or siTRPM7. (**D**) Immunolocalization of α-tubulin and ALIX at the midbody of siControl, siTRPV4 or siTRPM7 transfected HMEC. Bar= 5 μm. (**E**) Quantification of ALIX immunofluorescence intensities at the midbody. Data are means±SEM. Number of cells (or experimental repeats) indicated in each graph. Significance values are respect control condition as determined by Student's unpaired t test (B,C) or ANOVA followed by Dunnett's post hoc test (E).

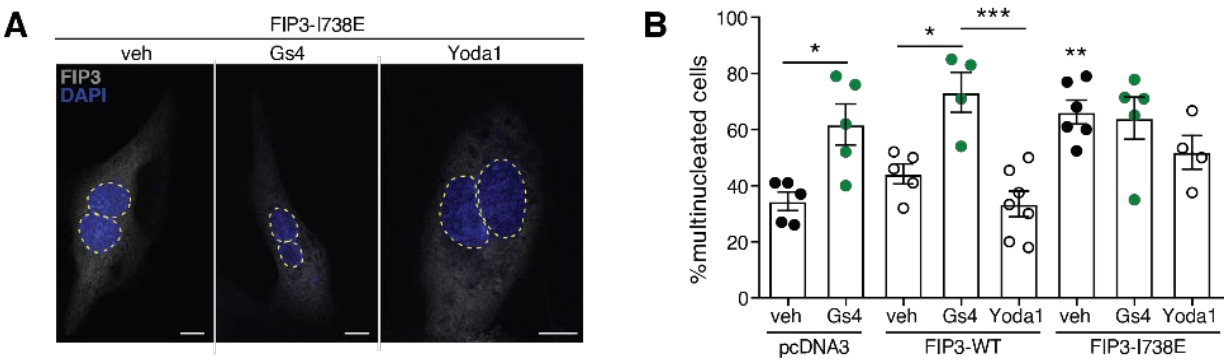

Fig. S11. Effect of FIP3 on HMEC multinucleation. (**A**) Nuclear staining of HMEC transfected with FIP3-I738E and treated with vehicle, GsMTx4 or Yoda1. Bar= 10 μm. (**B**) Multinucleation of HMEC overexpressing pcDNA3, FIP3-WT or FIP3-I738E in the presence or absence of GsMTx4. Data are means±SEM. Number of replicas indicated in each graph. Significance values are respect control condition as determined by ANOVA and Bonderroni's post hoc test.

Table S1.

Drugs, antibodies, oligonucleotides and plasmids used in this work

DRUG	SUPPLIER	TARGET	[µM]	INCUBATION	VEHICLE
GsTMx4	Alomone	Blocks Piezo1	4 1	Acute, Ca^{2+} imaging; 2h preincubation, time lapse/IF	H_2O
Yoda1	Tocris	Activates Piezo1	10-20 4	Acute, Ca^{2+} imaging; 2h preincubation, time lapse/IF	DMSO
HC067047	Tocris	Blocks TRPV4	0.1	Acute, Ca^{2+} imaging	DMSO
GSK1016790A	Sigma-Aldrich	Activates TRPV4	0.01 0,001	Acute, Ca^{2+} imaging, 2h preincubation, time lapse/IF	DMSO
FTY720	Sigma-Aldrich	Blocks TRPM7	10	Acute, Ca^{2+} imaging	DMSO
Naltriben	Sigma-Aldrich	Activates TRPM7	50 20	Acute, Ca^{2+} imaging; 2h preincubation, time lapse/IF	DMSO
Rockout	Calbiochem	Blocks Rho Kinase	5	2h preincubation, time lapse/IF	DMSO
Fura-2-AM	Life Technologies	Ratiometric Ca^{2+} indicator dye	5	30 min preincubation	DMSO
Calbryte™ 630 AM red	Deltaclon	Ca^{2+} indicator dye	5	30 min preincubation	DMSO
DAPI	Thermo	DNA, nuclear staining		1:1000; 10 min preincubation	1% BSA in PBS
Fluoromount G	Southern Biotech	Storage of slide preparations	NA	NA	H_2O
ANTIBODIES		**REFERENCE**	**CONCENTRATION**		
Rabbit polyclonal anti-Piezo1	Novus Biologicals	NBP1-78446	1:350 (5% BSA) for IF; 1:1000 for WB		
Mouse monoclonal anti-Piezo1	Novus Biologicals	NBP2-75617	1:1000 (5% milk) for WB		
Rabbit polyclonal anti-	Protein Tech	12303-1-AP	1:500 (5% BSA)		

ALG-2 (aka PDCD6)			
Rabbit polyclonal anti-CHMP4B	Sigma-Aldrich	HPA041401	1:300 (5% BSA)
Mouse Monoclonal Anti-αTubulin	Sigma-Aldrich	T6793	1:500 (5% BSA)
Mouse monoclonal anti-Pacsin3	Santa Cruz	sc-166923	1:1000 (5% BSA) 1:1000 (5% milk) for CoIP and WB
Goat anti-rabbit IgG AlexaFluor 647	ThermoFisher	A-21244	1:1000 (5% BSA)
Goat anti-mouse IgG AlexaFluor 555	ThermoFisher	A-21424	1:1000 (5% BSA)
Mouse monoclonal anti-α-Myc	Sigma-Aldrich	M4439	1:1000 (5% BSA) 1:1000 (5% milk) for CoIP and WB
Anti-GFP	Clontech	632380	1:1000 (5% BSA)
Peroxidase-conjugated anti-rabbit IgG	GE Healthcare	NA934	1:2000 (5% milk) 1:1000 (5% milk) for CoIP and WB
Secondary anti-mouse HRP	GE Healthcare	NXA931,	1:2000 (5% milk)
Rabbit polyclonal anti-ALIX	Cell Signaling	992880	1:350 (1% BSA)
Rabbit polyclonal anti-Cep55	GeneTex	GTX112190	1:350 (1% BSA)
Rabbit polyclonal anti-Rab11	Abcam	ab3612	1:350 (1% BSA)
Rabbit polyclonal anti-FIP3	Sigma-Aldrich	HPA028631	1:350 (1% BSA)
Rabbit polyclonal anti-Beclin1	Abcam	Ab62557	1:350 (1% BSA)
PLASMIDS		**REFERENCE**	
Human Piezo1-pIres-GFP		Provided by Dr. Frederick Sachs (University of Buffalo, USA) (*8*)	

Human Piezo1-P1578A/P1580A/P1584A/P1587A- pIres-GFP	Biomatik	
hPiezo1-WT-myc-IRES-GFP	Biomatik	
GenEPI		Dr.Periklis Pantazis, Imperial College London.
pcDNA3-Pacsin3-CFP	Own plasmid	Generated based on pcDNA3-myc-Pacsin3 provided by Markus Ploman (University of Cologne, Germany)
pCDNA3-Pacsin3-YFP	Own plasmd	Generated based on pcDNA3-myc-Pacsin3 provided by Markus Ploman (University of Cologne, Germany)
Rab11-WT-GFP	Addgene 12674	Dr. Ricardo Pagano (Mayo Clinic, Rochester, USA)
Rab11-Q70L-GFP	Addgene 49553	Dr. Marci Scidmore (University of Texas, USA)
Rab11-S25N-GFP	Addgene 12678	Dr. Ricardo Pagano (Mayo Clinic, Rochester, USA)
FIP3-GFP		Dr. Mary McCaffrey (University College Cork, Ireland)
FIP3-I738E-GFP		Dr. Mary McCaffrey (University College Cork, Ireland)
FIP3-4DA-GFP	Own plasmid	
EGFP-Rab35	Addgene 49552	Dr. Marci Scidmore (University of Texas, USA)
EGFP-Rab35-Q67L	Addgene 49612	Dr. Marci Scidmore (University of Texas, USA)
EGFP-Rab35-S22N	Addgene 49613	Dr. Marci Scidmore (University of Texas, USA)
mCherry-Tubulin-C18	Addgene 55148	Dr. Michael W Davison (Florida State University, USA)
pcDNA3.1-YFP-TRPM7		Dr. Thomas Gudermann (Ludwig-Maximilians Universität, Munich, Germany)
C-tail tagged hTRPV4-WT-GFP-His	Own plasmid	

MOLECULAR BIOLOGY TOOLS	**SUPPLIER**	**TARGET SEQUENCE (5′ to 3′)**
Control siRNA	Quiagen	AATTCTCCGAACGTGTCACGT
Piezo1 siRNA	Dharmacon	UCGCGGUGGUCGUCAAGUA

	Piezo1 5'UTR siRNA	Horizon	CGAAGGAGAAGGAGGAAGA
	Pacsin3 siRNA-1	Qiagen Pacsin3-6	GGACAUGGAACAGGCCUUU
	Pacsin3 siRNA-2	Dharmacon	CAGAGGACCATCAGCCGGCAAA
	PLKO.1-shRNA scramble	Dharmacon	Sense: TCCTAAGGTTAAGTTAAGTCGCCCTCG; Antisense: CGAGGGCGACTTAACCTTAGG
	PLKO.1-shRNA-Piezo1	Dharmacon	Sense: ATGATTGTACTTCTTGGTGAG; Antisense: CTCACCAAGAAGTACAATCAT
	Cep55 siRNA	Dharmacon	GTCCCAAGTGCAATATACAGTAT
	TRPV4 siRNA	Life Technologies	CCAAGUUUGUUACCAAGAU
	TRPM7 siRNA	Dharmacon	siRNA-SMART-pool cat nº M-005393-03-0005
	OLIGONULEOTIDES	**SEQUENCE (5′ to 3′)**	
	pEGFP-C1-FIP3-D215A/D217A/D219A/D247A (FIP3-4DA) Mutagenesis primers	Mutg1_Forward: GTTCGATGCCCTGGCCGGGGCTGGGGCCGGTTTCGTCCGCATC Mutg1_Reverse: GATGCGGACGAAACCGGCCCCAGCCCCGGCCAGGGCATCGAAC Mutg2_Forward: CTTAACTAAGTACTTGGCTCCCAGTGGGCTC Mutg2_ Reverse: GAGCCCACTGGGAGCCAAGTACTTAGTTAAG	
	Piezo1 SYBR green-based real time RT-PCR	Forward: TTCCTGCTGTACCAGTACCT Reverse: AGGTACAGCCACTTGATGAG	
	Pacsin3 SYBR green-based real time RT-PCR	Forward: GGACCTGGTCAGCTGCTTC Reverse: GCCTTCTCCAGTGTGCCATA	
	GADPH SYBR green-based real time RT-PCR	Forward: GGAGTCCACTGGCGTCTTC Reverse: TGGCTCCCCCTGCAAATG	
	TRPM7 SYBR green-based real time RT-PCR	Forward: TCTGCATTTGACCAGCTTATCC Reverse: TCTGCATTTGACCAGCTTATCC	

	TRPV4 SYBR green-based real time RT-PCR	Forward: CCCGTGAGAACACCAAGTTT Reverse: GTGTCCTCATCCGTCACCTC